Distributed-Force Recovery for a Planar Photoelastic Tactile Sensor

Ricardo E. Saad, *Student Member, IEEE,* Adi Bonen, Kenneth C. Smith, *Fellow, IEEE,* and Beno Benhabib, *Member, IEEE*

***Abstract*—In this paper, an efficient force-recovery algorithm is presented for a novel planar photoelastic tactile transducer. A distributed-force profile input to the tactile sensor developed in our laboratory generates stress in the photoelastic layer of the transducer, making it birefringent. Circularly polarized light input to the transducer is elliptically polarized at the output due to phase-lead created in the stressed photoelastic layer. The algorithm presented recovers the phase-lead distribution and correlates it to the input force profile. Since this distribution is a linear function of the force profile, the solution of the inverse-tactile problem is significantly simplified. The paper presents the analytical basis of the algorithm as well as the numerical technique used in its solution.**

I. Introduction

CURRENT methods of tactile-force transduction include piezoelectric, piezoresistive, capacitive and optical techniques [1]–[3]. Among optical methods, there exists a strong possibility that photoelastic tactile sensors could be implemented in the near future by using integrated optics and optoelectronics, in a manner analogous to piezoresistive tactile transducers that are presently implemented using micromachining and microelectronics.

The few studies that have been published on photoelastic tactile sensors include the description of a basic transducer [4], [5], and a theoretical model used to analyze it [6]. Research results presented in these papers clearly show that photoelastic transducers can satisfy many of the tactile-sensing requirements specified in [7]. In an earlier work [8], although the researchers were successful in developing a photoelastic force sensor, their transducer cannot be adapted directly for tactile sensing.

Photoelastic sensors have also been developed to detect slippage. One such sensor, described in [9], uses a transducer similar to the one described in [4], [5]; however, in this case, the analysis of the fringes is used only to detect movement of the grasped object. For this type of application, a special technique was reported in [10] to optimize the comparison process for detecting differences between two fringe patterns, occurring due to the slippage of the grasped object.

Manuscript received April 24, 1995; revised November 16, 1995. This work was supported by the Natural Sciences and Engineering Research Council of Canada, and CNPq, Brazil.

R. E. Saad is with the Computer Integrated Manufacturing Laborabory (CIMLab), University of Toronto, Toronto, Ontario, Canada M5S 1A4.

A. Bonen and K. C. Smith are with the Department of Electrical and Computer Engineering, University of Toronto, Toronto, Ontario, Canada M5S 1A4.

B. Benhabib is with the Department of Mechanical Engineering, University of Toronto, Toronto, Ontario, Canada M5S 1A4.

Publisher Item Identifier S 0018-9456(96)02492-8.

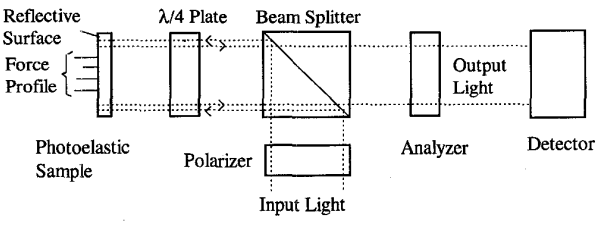

Fig. 1. A circular reflective polariscope.

Almost all of the photoelastic sensors developed thus far for robotics use a polariscope for illuminating and collecting the light from the photoelastic transducer. The polariscopes can be either linear or circular, depending on the required polarization of the light. They can also be characterized as a reflective or a transparent type, depending on whether the photoelastic transducer reflects or transmits the light.

A circular, reflective polariscope is shown in Fig. 1. The input light is linearly polarized and then directed toward the photoelastic transducer by a beam splitter. Before reaching the transducer the light is circularly polarized by a quarter-wave plate. Once the light penetrates the transducer, its polarization is affected by the birefringence induced in the photoelastic element by the forces applied to the transducer. The birefringence creates a phase-lead distribution that transforms the circularly polarized light into elliptically polarized light. A reflective surface on the back side of the transducer returns the light toward a detector through the quarter-wave plate, the beam splitter and an analyzer. The output light intensity distribution consists of a fringe pattern, which will be further discussed in Section III.

The photoelastic tactile transducer developed in our laboratory was first presented in [11]. It utilizes a circular, reflective polariscope. In this paper, an algorithm that accurately and effectively determines the phase-lead distribution from a noisy light-intensity distribution is presented. While this algorithm was created for an improved version of this transducer, it must be noted that it is also applicable to other photoelastic sensors, e.g., [6]. As will be shown in Section III, the reason for recovering the force profile from the phase-lead distribution, rather than from the light-intensity distribution, is that the phase-lead distribution is a linear function of the force profile. The recovery of the phase-lead distribution constitutes the first step in solving the inverse-tactile problem. A solution for this

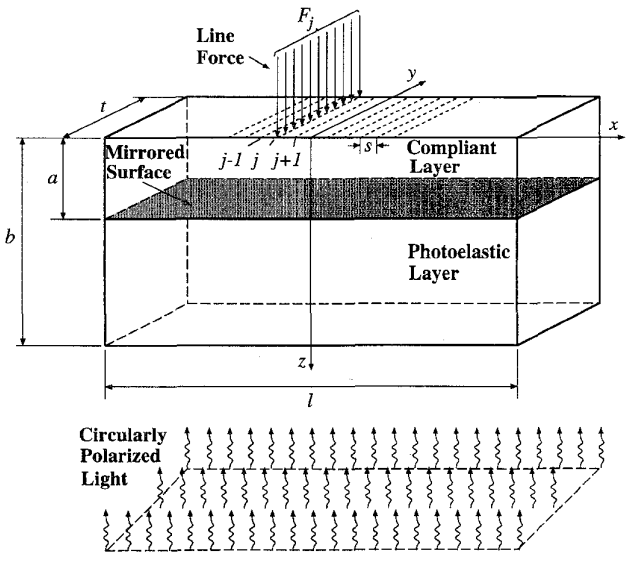

Fig. 2. Two-layer photoelastic transducer.

problem is also presented herein. As well, the transduction model used allows the formation of closed-form equations for both the light-intensity distribution and the phase-lead distribution.

II. The Transducer

The proposed transducer consists of a fully supported two-layer beam with a mirrored surface sandwiched in between, Fig. 2. It is assumed that a set of normal line-distributed forces is applied to the top surface of the beam. The forces are applied at discrete tactels separated by equal distances, s, along the beam. The upper "compliant" layer is for the protection of the mirror, while the lower one is the photoelastic layer.

Circularly polarized monochromatic light, incident along the z-axis, illuminates the bottom surface of the transducer. The light propagates parallel to the z-axis, passes through the photoelastic layer, and then reflects back from the mirror. If no force is applied to the transducer, the returning light is circularly polarized since the unstressed photoelastic material is isotropic. If force is applied, stresses are induced in the photoelastic layer, making the material birefringent. This introduces a certain phase-difference (a phase-lead) between the components of the electric field associated with the light-wave propagation in the two allowed directions of polarization [12]. The two directions of polarization are in the plane perpendicular to the direction of propagation, in our case the x–y plane. As a consequence of this effect, the output light is elliptically polarized, creating a phase-lead distribution, p, between the input light and the output light at each point in the x–y plane.

III. Phase-Lead Distribution

In order to determine the phase-lead distribution, it is assumed that stresses in the transducer can be calculated by the plane-stress approximation described in [6], [13]. This model allows us to analyze the behavior of the transducer by using closed-form equations in which the phase-lead is only a function of x. The total phase-lead is the summation (integral) of all the phase-leads introduced at different points of the photoelastic layer along the z-coordinate.

Let F_j, shown in Fig. 2, be the magnitude of the force applied at the jth (discrete) position (tactel). The phase-lead distribution, p_j, can then be calculated as

$$p_j(x) = \frac{4K_{ss}}{\lambda t}\left[\frac{a^2}{(x-x_j)^2+a^2} - \frac{b^2}{(x-x_j)^2+b^2}\right]F_j \quad (1)$$

where K_{ss} is the stress optical coefficient, t is the width of the photoelastic transducer, a is the thickness of the compliant layer, b is the thickness of the transducer, x_j is the x-coordinate of the jth tactel, and λ is the wavelength of the input light.

For a set of forces applied at n tactels, the total phase-lead distribution is given by

$$p(x) = \sum_{j=1}^{n} p_j(x) = \sum_{j=1}^{n} \psi_j(x)F_j \quad (2)$$

where

$$\psi_j(x) = \frac{4K_{ss}}{\lambda t}\left[\frac{a^2}{(x-x_j)^2+a^2} - \frac{b^2}{(x-x_j)^2+b^2}\right]. \quad (3)$$

Equation (2) is obtained by applying the principle of superposition. Correspondingly, the phase-lead distribution is a linear function of the applied forces.

The normalized light-intensity distribution at the output of the polariscope is given by [6]

$$I(x) = \sin^2\frac{p(x)}{2}. \quad (4)$$

One can note that the major problem that exists in inverting (4) is the possibility that $p(x) \leq -\pi$ for some $-l/2 \leq x \leq l/2$.

The first step in the proposed algorithm for the recovery of $p(x)$ from $I(x)$ is, thus, the classification of the critical points of $I(x)$ as follows [11]:

a) *Class 1* consists of critical points of $I(x)$, where $I(x) = 1$ and the first nonnegative derivative is of the form $d^{2k+1}I/dx^{2k+1}$ for some integer $k \geq 1$.
b) *Class 2* consists of critical points of $I(x)$, where $I(x) = 0$ and the first nonnegative derivative is of the form $d^{2k+1}I/dx^{2k+1}$ for some integer $k \geq 1$.
c) *Class 3* consists of critical points of $I(x)$, which are local extrema but do not satisfy conditions a) or b).

For the second step of the algorithm, it is assumed that $p(l/2) \geq -\pi$. Then, the phase-lead distribution can be reconstructed using the formula

$$p(x) = -2\pi M - (-1)^{M+N}2\arcsin\sqrt{I(x)} \quad (5)$$

where $M \rightarrow M + (-1)^K$.

The iterative algorithm starts with $M = 0$, $N = 0$, and $K = 0$. The phase-lead distribution is recovered point-by-point, increasing x from $-l/2$–$l/2$. When a *Class-3* critical

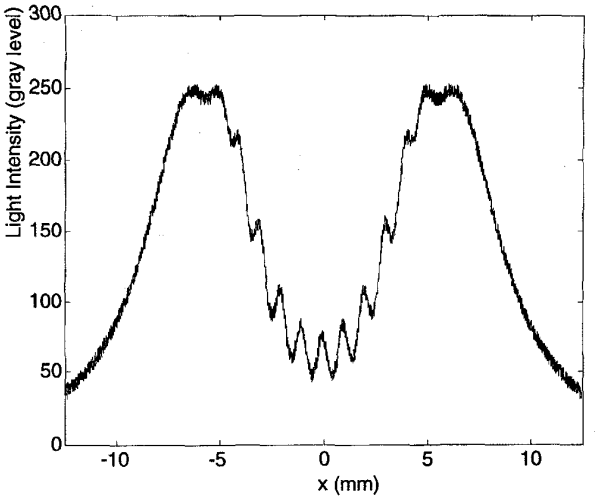

Fig. 3. Detected light-intensity distribution in gray levels.

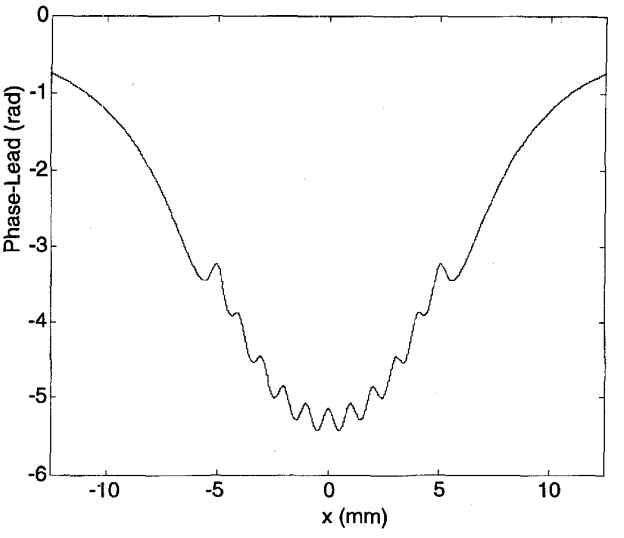

Fig. 4. Phase-lead distribution.

point is encountered, K is increased by one; when a *Class-2* critical point is encountered, N is increased by one; and, when a *Class-1* critical point is encountered, M is increased or decreased by one depending on the value of K.

IV. Noise and Quantization Error

It is assumed that light originating from the polariscope is detected by a CCD linear array having an active length equal to the length of the transducer and set parallel to the x coordinate. Since the linear array samples the light-intensity distribution in pixel-quantized space, Equation (4) can be rewritten in a discrete form as

$$I(x_i) = \sin \frac{p(x_i)}{2} \quad \text{for} \quad i = 1, 2, \cdots, m \tag{6}$$

where m is the number of pixels of the linear array.

The equations for $p(x)$ and $\psi_j(x)$, (2) and (3), respectively, can also be rewritten in a discrete form as

$$P_i = p(x_i) \quad \text{for} \quad i = 1, 2, \cdots m \tag{7}$$

$$\psi_{ij} = \psi_j(x_i) \quad \text{for} \quad i = 1, 2, \cdots, m \quad j = 1, 2, \cdots, n. \tag{8}$$

The discrete version of (2) can, thus, be rewritten using a matrix notation as

$$\boldsymbol{P} = \boldsymbol{\Psi F} \tag{9}$$

where $\boldsymbol{P}$ is the $(m \times 1)$ phase-lead vector, $\boldsymbol{\Psi}$ is the $(m \times n)$ base matrix, and $\boldsymbol{F}$ is the $(n \times 1)$ input force vector.

Once the light intensity has been discretized by the linear CCD array, the measurements are converted into digital form by an A/D converter. The A/D converter introduces quantization error in addition to the random electronic noise that would be present due to the detection process. Correspondingly, the detected light-intensity distribution (in gray levels), I_d, can be written as

$$I_d(x_i) = \text{round}\left[A \sin^2 \frac{p(x_i)}{2} + n_o(x_i) + I_o\right] \quad \text{for} \quad i = 1, 2, \cdots, m \tag{10}$$

where n_o is the total noise introduced into the measurement; I_o is the minimum average voltage applied to the A/D converter, such that $[I_o + \min(n_o)] \geq 0$; and A is the maximum allowed dynamic range of the A/D converter, such that $[A + I_o + \max(n_o)] \leq [2^B - 1]$ (where B is the number of bits in the A/D converter). The "round" function returns the closest integer to the real number presented to it.

Now, the phase-lead distribution has to be recovered from (10). However, the critical points of I_d cannot be classified using the algorithm outlined in Section III, since the derivatives of I_d cannot be calculated accurately. Thus, a modified algorithm that allows us to recover the phase-lead distribution from a noisy light-intensity distribution has been developed as reported in the next section.

V. Recovering the Phase-Lead from Noisy Data

For clarity purposes, the proposed algorithm is explained herein via an example. For the example, the parameters and dimensions of the transducer, the A/D converter and the linear array are as follows: $a = 0.5$ mm, $b = 3$ mm, $t = 2$ mm, $l = 250$ mm, $s = 1$ mm, $\lambda = 632.8$ nm, $E = 0.004$ GPa, $K_{ss} = 1.70 \times 10^{-9}$ m^2/N, $\nu = 0.5$, $B = 8$ bits, $m = 2048$, $n = 11$, $I_o = 5$, and $A = 245$. The noise n_o is assumed to be random and limited between -5 and 5 gray levels. Further, it is assumed that each tactel of the transducer is subjected to the same force, namely $F_j = 0.1$ N for $j = 1, 2, \cdots, 11$. Fig. 3 shows the noisy light-intensity distribution corresponding to the phase-lead distribution caused by the input force, Fig. 4.

A description of the modified algorithm follows.

a) The light-intensity distribution is filtered with an ideal low-pass filter. The noise, in our example, was reduced to the range of -2–2 gray levels, from -5–5 by utilizing a passband of 200 μm^{-1}.

b) The filtered light-intensity distribution is normalized, Fig. 5, and the critical points are identified; in our example these are c_k, $k = 1, 2, \cdots, 25$.

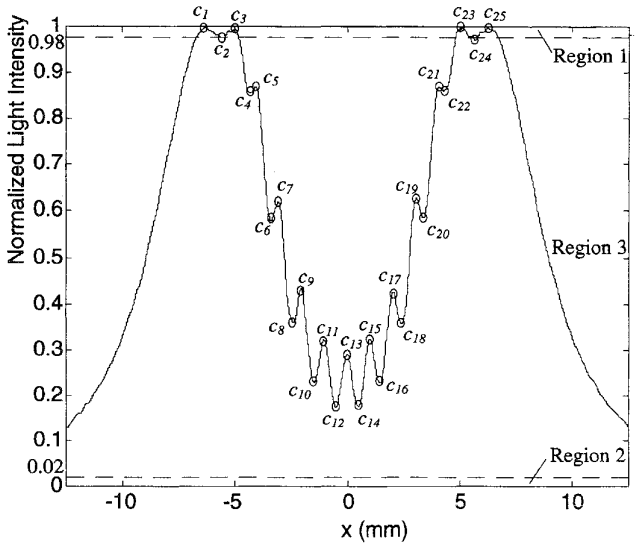

Fig. 5. Normalized light-intensity distribution.

It is verified that two consecutive critical points do not occur "too close" to each other, since such closely paired critical points would imply a noisy observation. The threshold value for "closeness" was chosen as 20 pixels for the example.

c) Three regions are defined in the normalized light-intensity distribution for the classification of the critical points, Fig. 5. In our example, on the normalized intensity scale, Region 1 is defined as $0.98 \leq I \leq 1$, Region 2 as $0 < I < 0.02$ and Region 3 as $0.02 \leq I \leq 0.98$. The widths of Regions 1 and 2 were obtained approximately by dividing the maximum error in the filtered light-intensity distribution by A (that is, 4/245 $\sim$ 0.02).

The critical points are now classified as follows:

1) All *local extrema* in Region 1 are either *Class-1* or *Class-3* critical points. In our example, c_1, c_2, c_3, c_{23}, and c_{25} are in Region 1.
2) All *local extrema* in Region 2 are either *Class-2* or *Class-3* critical points. In our example, there are no critical points in Region 2.
3) All *local extrema* in Region 3 are *Class-3* points. In our example, c_k for $k = 4, 5, \cdots, 22$ and c_{24} are in Region 3.

Due to uncertainties about the class of critical points in Regions 1 and 2, several different phase-lead distributions can be recovered using (5), of which only one is correct. Each local extremum in Regions 1 and 2 would yield two possible phase-lead distributions. If the total number of local extrema in Regions 1 and 2 is C, then the total number of possible phase-lead distributions is 2^C. In our example $C = 5$, leading to 32 possibilities.

d) The number of possible phase-lead distributions is reduced. To accomplish this objective, all the possible cases are checked with respect to a set of heuristics.

1) *Rule 1:* If c_{k1} and c_{k2} are both *Class-1* or both *Class-2* critical points, such that between them only *Class-3* critical points exist, then the number of such *Class-3* critical points must be odd.

TABLE I
REDUCED SET OF POSSIBLE CRITICAL POINTS

Case #	c_1	c_2	c_3	c_k (k=4,5...22)	c_{23}	c_{24}	c_{25}
1	0	0	0	0	0	0	0
2	0	0	0	0	1	0	1
3	0	0	1	0	0	0	1
4	0	0	1	0	1	0	0
5	1	0	0	0	0	0	1
6	1	0	0	0	1	0	0
7	1	0	1	0	0	0	0
8	1	0	1	0	1	0	1

2) *Rule 2:* If c_{k1} is a *Class-1 (Class-2)* critical point and c_{k2} is *Class-2 (Class-1)* critical point, such that between them only *Class-3* critical points exist, then the number of such *Class-3* critical points must be even.
3) *Rule 3:* If c_{k1} and c_{k2} are two consecutive critical points, they cannot be both *Class-1* or both *Class-2* critical points.
4) *Rule 4:* The parameter M in (5) must be zero for $x = -l/2$ and $x = l/2$. This implies certain symmetry in the distribution of critical points.

Applying the above verification rules to the set of 32 possible cases in our example, the possible set of phase-lead distributions was reduced to 8. For coding purposes, the number "1" is assigned to *Class 1*, "−1" to *Class 2* and "0" to *Class 3*, as shown in Table I.

e) The phase-lead distribution, $\boldsymbol{P}_r$, is recovered, using the procedure described in Section III, for each case shown in Table I.

f) The spurious phase-lead distributions are eliminated, since only one of the solutions in the reduced set is correct.

To achieve this objective, all the force profiles, $\boldsymbol{F}_r$, corresponding to the limited set of potential phase-lead distributions, $\boldsymbol{P}_r$, must be found by solving (9).

A similar problem was addressed in a previous study for the case of a piezoresistive tactile sensor [14]. Therein, a neural network was proposed to solve the inverse-tactile problem. In our case, the following nonnegative least-squares (nnls) problem was formulated and solved

$$\min_{F_r} ||\boldsymbol{\Psi F}_r - \boldsymbol{P}_r||, \quad \text{such that} \quad \boldsymbol{F}_r \geq 0 \tag{11}$$

where $\boldsymbol{\Psi}$ and $\boldsymbol{P}_r$ are the coefficients of the objective function. (The vector $\boldsymbol{F}_r$ is restricted to be nonnegative due to the positive-force-profile requirement in our case).

In our example, for Case 1 in Table I, the following force profile was recovered using (11)

$$\boldsymbol{F}_r = (0.2156,\ 0.0868,\ 0,\ 0,\ 0,\ 0,\ 0,\ 0,\ 0,\ 0.0860,\ 0.2161)\,\text{N}.$$

g) The recovered force profiles obtained by solving (11) are verified via (9). Let $\boldsymbol{P}_v$ be the phase-lead distribution obtained when the estimated force profile $\boldsymbol{F}_r$ is applied to (9)

$$\boldsymbol{P}_v = \boldsymbol{\Psi F}_r. \tag{12}$$

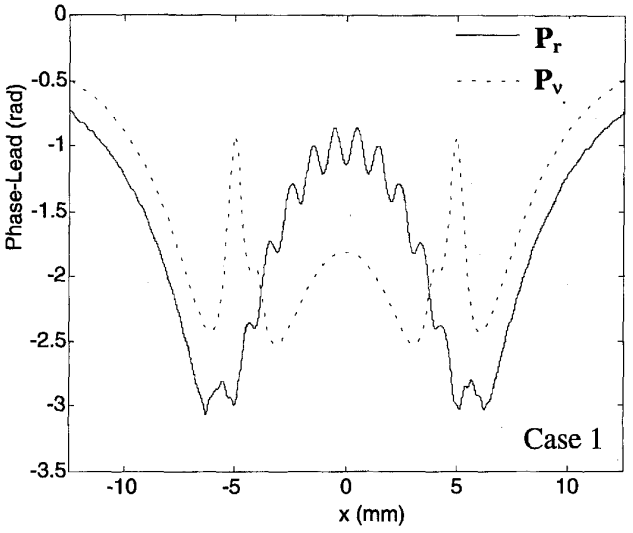

Fig. 6. Phase-lead distributions $\boldsymbol{P}_r$ and $\boldsymbol{P}_v$ for Case 1.

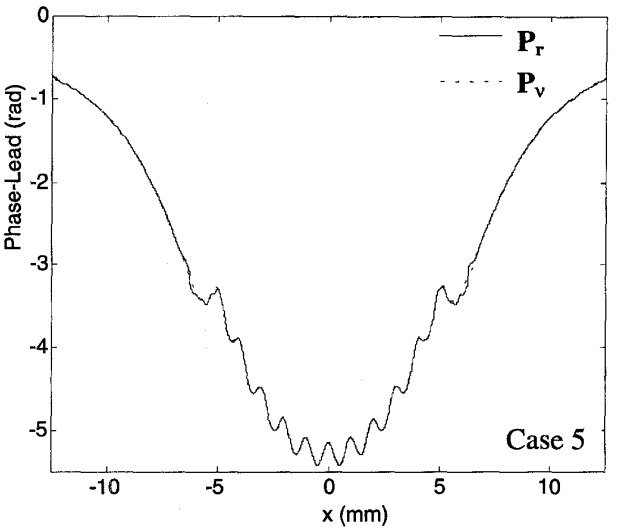

Fig. 7. Phase-lead distributions $\boldsymbol{P}_v$ and $\boldsymbol{P}_r$ for Case 5.

For the correct estimate of $\boldsymbol{F}_r$ the difference between $\boldsymbol{P}_r$ and $\boldsymbol{P}_v$ must be minimal due to the least-squares fit.

Let a normalized error be defined, for each case, as

$$\text{Error}(\%) = \frac{1}{\Delta \text{P}_{\max}} \max\{\text{abs}\,[\boldsymbol{P}_v - \boldsymbol{P}_r]\} \times 100 \qquad (13)$$

where the function $\hat{\text{abs}}$ calculates the absolute value of each component of the difference between the vectors $\boldsymbol{P}_r$ and $\boldsymbol{P}_v$, and $\Delta P_{\max}$ is the difference between the overall absolute maximum and minimum values of $\boldsymbol{P}_r$ and $\boldsymbol{P}_v$.

In Fig. 6, both $\boldsymbol{P}_r$ and $\boldsymbol{P}_v$ are plotted for Case 1. As can be observed, there exists a large difference between the two phase-lead distributions. This correctly implies that Case 1 is not the true phase-lead distribution.

The correct phase-lead distribution is the one that corresponds to Case 5, as shown in Fig. 7. The normalized error for this case is 3.2%. (Table II shows the normalized errors for all eight cases considered). The recovered force profile for Case 5 is

$$\boldsymbol{F}_r = (0.0994,\ 0.1017,\ 0.1004,\ 0.1002,\ 0.0987,\ 0.0994,\ 0.0996,\ 0.1006,\ 0.1011,\ 0.1019,\ 0.0972)\,\text{N}.$$

When one compares the above $\boldsymbol{F}_r$ with the true input $F_j = 0.1$ N, $j = 1, 2, \cdots, 11$, the maximum error component in force recovery is determined to be 1.9%.

TABLE II
NORMALIZED ERRORS FOR ALL CASES SHOWN IN TABLE I

Case #	*1*	*2*	*3*	*4*	*5*	*6*	*7*	*8*
Error(%)	42.9	40.6	9.6	9.4	3.2	10.1	40.9	40.6

VI. CONCLUSIONS

In this paper, a general algorithm has been presented for the automatic recovery of the phase-lead distribution for a photoelastic tactile sensor. The noisy light-intensity distribution is assumed to be detected by a CCD linear array camera linked to an A/D converter. The algorithm takes into account the random noise generated by the electronic circuits of the camera, as well as the quantization error generated by the A/D converter.

Some simulation results using a two-dimensional optomechanical model were presented to verify the proposed algorithm. To solve the inverse tactile problem an optimization function was successfully implemented.

In practice, finding the correct phase-lead distribution might, in some cases, be computationally time-consuming if each distribution is considered sequentially. This is a consequence of the complexity of the algorithm by which the inverse-tactile problem must be solved. However, one can process the different phase-lead distributions in a parallel manner. Use of dedicated hardware to solve the inverse tactile problem, such as the one proposed in [14] for instance, is particularly attractive.

REFERENCES

[1] H. R. Nicholls and M. H. Lee, "A survey of robot tactile sensing technology," *Int. J. Robot. Res.*, vol. 8, no. 3, pp. 3–30, 1989.
[2] R. A. Russell, *Robot Tactile Sensing*. Brunswick, Australia: Prentice Hall, 1990.
[3] H. R. Nicholls, Ed., *Advanced Tactile Sensing for Robotics*. Singapore: World Scientific, 1992.
[4] A. Cameron, R. Daniel, and H. Durrant-Whyte, "Tactile geometry for images and normals," in *Tactile Sensing and the Photoelastic Tactile Sensor*, Tech. Rep. OUEL 1758/89, Department of Engineering Science, University of Oxford, UK, pp. 1–16, 1989.
[5] K. W. Loh, H. Durrant-Whyte, and R. Daniel, "A photoelastic tactile sensor," Tech. Rep. OUEL 1792/89, Department of Engineering Science, University of Oxford, UK, 1989.
[6] A. Cameron, R. Daniel, and H. Durrant-Whyte, "Touch and motion," in *IEEE Int. Conf. Robotics and Automation*, Philadelphia, 1988, pp. 1062–1067.
[7] L. D. Harmon, "Automated tactile sensing," *Int. J. Robot. Res.*, vol. 1, no. 2, pp. 3–32, 1982.
[8] S. C. Jacobsen, J. E. Wood, D. F. Knutti, and B. Biggers, "The Utah/MIT dextrous hand: Work in progress," in *Robotic Research: The First International Symposium*, M. Brady and R. Paul, Eds. Cambridge: The MIT Press, 1983, pp. 601–653.

[9] F. Eghtedari and C. Morgan, "A novel tactile sensor for robot applications," *Robotica,* vol. 7, pp. 289–295, 1989.
[10] S. H. Hopkins, F. Eghtedari, and D. T. Pham, "Algorithms for processing data from a photoelastic slip sensor," *Mechatronics,* vol. 2, no. 1, pp. 15–28, 1992.
[11] R. E. Saad, B. Benhabib, and K. C. Smith, "A novel photoelastic tactile transducer for robotics," in *SME Fifth World Conf. Robotics Research,* Cambridge, MA, 1994, pp. 4:1–14.
[12] K. Iizuka, *Engineering Optics,* 2nd ed. Berlin: Springer-Verlag, 1987.
[13] R. S. Fearing and J. M. Hollerbach, "Basic solid mechanics for tactile sensing," *Int. J. Robot. Res.,* vol. 4, no. 3, pp. 40–54.
[14] Y. C. Pati, "Neural networks for low level processing of tactile sensory data," Master's Thesis, Dept. Electrical and Computer Engineering, University of Maryland, College Park, 1989.

Ricardo E. Saad (S'95) received the electrical engineering diploma with first class honors from the National University of Cordoba, Argentina, in 1986 and the M.Sc. degree with distinction award in electrical engineering from the State University of Campinas (UNICAMP), Brazil, in 1989. He is currently a Ph.D. candidate in the Department of Electrical and Computer Engineering, University of Toronto, Toronto, Ontario, Canada.

From 1987 to 1990, he was with the Optoelectronics Device Department, Research Center, Brazilian Telecommunication Holding Company (CPqD-Telebras). Since 1991, he has been with the Computer Integrated Manufacturing Laboratory (CIMLab), University of Toronto. His interests are in robotic sensing, optical sensing, optoelectronics, and microwave and optical telecommunications.

Adi Bonen was born on November 3, 1963, in Israel. He graduated Summa Cum Laude from the Technion, Israel Institute of Technology, with the B.A.Sc. degree in electrical engineering in 1990. Since 1990, he has been a Ph.D. student in the Department of Electrical and Computer Engineering, University of Toronto. During 1992–1993, he was on a research-internship program at the Hitachi Central Research Laboratories, Tokyo, Japan, working on an optical computed-tomography system. His current research interests include electro-optical measurements, robotic sensors, and sensing techniques.

Kenneth C. Smith (F'78) obtained the Ph.D. degree in solid-state physics in 1960 from the University of Toronto, where he is presently a Professor of Electrical Engineering, Mechanical Engineering, Computer Science, and Library and Information Science.

He was a Visiting Professor at the Department of Electrical and Electronic Engineering, Hong Kong University of Science and Technology, Kowloon, from 1993 to 1995. He has extensive industrial experience in the design and application of computers and electronic circuits, as employee, manager, administrator, entrepreneur, consultant, and educator. His research interests currently include analog VLSI, multiple-valued logic, sensor systems, machine vision, instrumentation, array architectures, human factors, and reliability. He is widely published in these and other areas, with more than 200 journal and proceedings papers, books, and book contributions.

Dr. Smith was elected Fellow of the IEEE in 1978 for "Contributions to Digital Circuit Design," and Honorary Professor at the Shanghai Institute for Railway Technology in 1989.

Beno Benhabib (M'93) is an Associate Professor in the Department of Mechanical Engineering, University of Toronto. His research interests are in the area of computer integrated manufacturing.

He is a member of the ASME, SME, AAAI, and a registered Professional Engineer in the Province of Ontario, Canada.